Journal of Luminescence 154 (2014) 185–192

Contents lists available at ScienceDirect

Journal of Luminescence

journal homepage: www.elsevier.com/locate/jlumin

White light generation from YAG/YAM:Ce^{3+}, Pr^{3+}, Cr^{3+} nanophosphors mixed with a blue dye under 340 nm excitation

J. Oliva [a], E. De la Rosa [a,*], L.A Diaz-Torres [a], A. Torres [b], P. Salas [c], O. Meza [d]

[a] Centro de Investigaciones en Optica, A.P. 1-948, León, Gto 37150, México
[b] Universidad Autónoma de Nuevo León, A.P. 126-F, Monterrey, NL 66450, México
[c] Centro de Física Aplicada y Tecnología Avanzada, Universidad Nacional Autónoma de México, A.P. 1-1010, Juriquilla, Qro. 76000, México
[d] Benemérita Universidad Autónoma de Puebla, 4 Sur 104 Centro Historico, 72000 Puebla, México

ARTICLE INFO

Article history:
Received 25 October 2013
Received in revised form
22 March 2014
Accepted 15 April 2014
Available online 24 April 2014

Keywords:
YAG
White light
Cerium
Praseodymium
Nanophosphors
Dye

ABSTRACT

The structural and luminescent properties of $Y_3Al_5O_{12}/Y_4Al_2O_9:Ce^{3+}$(0.1%)–$Pr^{3+}$(0.1%) –$Cr^{3+}$ (trace impurities) nanophosphors synthesized by a simple hydrothermal method were studied. The crystalline phase was composed of Yttrium Aluminum Garnet (YAG) and Yttrium Aluminum Monoclinic (YAM) depending on the ammonia concentration and annealing temperature. Ammonia increased the stabilization of YAG from 55 wt% to 63 wt% in the samples annealed at 900 °C, and an increment of 83% of the overall emission under 460 nm excitation was observed. Quenching of the emitted signal after annealing at 1100 °C was observed in spite of single YAG crystalline phase stabilization, due to the formation of Ce^{4+}, Pr^{4+}, and color centers. In addition to the green–yellow emission from Ce^{3+}, all samples present a broad red emission band produced by the relaxations from the broad band $^4T_2$ toward the $^4A_2$ energy level of Cr^{3+} impurities, under 340 nm excitation. By taking advantage of this broad green–yellow–red emission and using a blue dye, white light with CIE coordinates of (0.30, 0.36) under 340 nm excitation was produced.

1. Introduction

Trivalent cerium doped YAG phosphors ($Y_3Al_5O_{12}:Ce^{3+}$) have demonstrated their reliability for applications in discharge lamps and phosphor converted light emitting diodes (pc-LEDs) to produce white light [1,2]. However, the commercial YAG:Ce^{3+} based LEDs present a low color rendering index (CRI < 80) because the red component is poor. Some research groups have been working to incorporate this red component as well as to reach the optimal CIE (Commission Internationale d'Eclairage) coordinates of (0.33, 0.33) by codoping with rare earth (RE) the YAG:Ce^{3+} nanophosphors. Several ions have been used for this purpose; Gd^{3+} induces a little shift of yellow emission to longer wavelengths, and Eu^{3+}, Sm^{3+}, Pr^{3+}, Tb^{3+} produce a weak red emission after excitation at 470 nm [3,4]. The CRI was improved to 80 by using Tb^{3+}, and 83 by using Pr^{3+} and annealing temperature of 1500 °C [5–7]. For Pr^{3+}, the red emission was the result of energy transfer from Ce^{3+} (donor) to Pr^{3+} (acceptor) taking advantage that acceptor has its $^3P_0$ levels in resonance with the 5d levels of cerium [7]. However, strong red emission of Pr^{3+} has been reported in hosts such as $BaMoO_4$ and $CaTiO_3$ by direct excitation at 450 nm and 330 nm respectively [8,9]. Optimization of red emission has also been explored by modifying the synthesis process, solid-state reaction, combustion method and polyol method, drying process and annealing temperature. Some problems derived from those procedures are the high temperatures of synthesis as well as the weak red contribution to YAG:Ce^{3+} emission.

To overcome those problems discussed above and to improve the red emission, it is reported in this paper the synthesis of YAG/YAM:Ce^{3+}, Pr^{3+}, Cr^{3+} nanophosphors by using the well-known hydrothermal process which also permits low cost and capabilities to large scale production of phosphors [10,11]. In this paper, the effect of ammonia (NH_4OH) on the luminescent properties of YAG/YAM:Ce^{3+}, Pr^{3+}, Cr^{3+} under the excitation wavelengths of 340 nm or 460 nm is reported. The aims of this study are: (1) to demonstrate how the introduction of ammonia could increase the red component of the overall emission in YAG/YAM:Ce^{3+}, Pr^{3+}, Cr^{3+} nanophosphors when excited with 460 nm; (2) to show the emission of a broad red band of Pr^{3+} superposed to the yellow emission of Ce^{3+} when the YAG/YAM:Ce^{3+}, Pr^{3+}, Cr^{3+} nanophosphors are excited at 340 nm; and (3) to show white light emission with CIE coordinates (0.30,0.36) produced by the overlapping of the green–yellow–red light of the YAG/YAM:Ce^{3+}, Pr^{3+}, Cr^{3+} nanophosphors and the blue light of a dye under excitation at 340 nm.

* Corresponding author.
E-mail address: elder@cio.mx (E. De la Rosa).

http://dx.doi.org/10.1016/j.jlumin.2014.04.018
0022-2313/

2. Experimental

2.1. Synthesis of YAG/YAM:Ce^{3+}, Pr^{3+}, Cr^{3+}

All the chemical precursors $Y(NO_3)_3 \cdot 5H_2O$, $Al(NO_3)_3 \cdot 5H_2O$, $Ce(NO_3)_3 \cdot 5H_2O$, $Pr(NO_3)_3 \cdot 5H_2O$ and cetyltrimethylammonium bromide (CTAB) were acquired from Aldrich Inc. and ammonia (NH_4OH) was purchased from Karal; all precursors were used without further treatment. The YAG/YAM:Ce^{3+}, Pr^{3+}, Cr^{3+} nanophosphors co-doped with 0.1 mol% of Ce_2O_3, 0.1 mol% of Pr_2O_3, were synthesized by a hydrothermal process. Fourteen samples were prepared by using sodium hydroxide (NaOH) as precipitant agent and ammonia (NH_4OH) was added in six of them. In this procedure, all nitrates and CTAB (5 wt%) used as surfactant to avoid conglomeration of nanoparticles were mixed in distilled water at room temperature under vigorous stirring; subsequently, the precipitation was achieved with a solution (4 M) of sodium hydroxide added by slow dropping. Ammonia was added after adding the solution of NaOH. Thereafter, the resulting solution was transferred into a sealed stainless autoclave, which was maintained at 100 °C during 12 h. The precipitate was washed with distilled water and ethanol several times and dried in an oven at 100 °C for 12 h. Finally, the samples were annealed in air at 900 °C and 1100 °C for 3 h, with a heating rate of 5 °C/min. Table 1 summarizes the composition and main parameters of synthesis of the fourteen samples. Samples C1 and C2 were obtained by impregnating sample N1 with coumarin 480 as explained in Section 2.4. It is worthy to mention that during the synthesis of YAG/YAM:Ce^{3+}, Pr^{3+} trace impurities of Cr^{3+} appeared. Those impurities came from the corrosion of the stainless autoclave used for synthesis, since the pH used for synthesis after adding ammonia was 12, which is able to produce degradation of the stainless autoclave. It was not possible to detect those trace impurities using conventional methods as explained later.

2.2. Crystalline structure and morphology

The crystalline phase of the nanophosphors was determined by X-ray diffraction (XRD) using a SIEMENS D-5005 diffractometer with a Cu tube with Kα radiation at 1.5405 Å, scanning in the 25–80° (2θ range) with increments of 0.02° and a swept time of 2 s. In addition, the morphology and crystalline structure of prepared samples were performed in a High Resolution Transmission Electron Microscope (HRTEM), FEI-Titan 80–300 keV. The microscope is equipped with an ultra stable Schottky-type field emitter gun. The samples were grounded, suspended in isopropanol at room temperature, and dispersed with ultrasonic agitation; then, an aliquot of the solution was dropped on a 3 mm diameter lacey carbon copper grid. Electron diffraction scattering (EDS) was also achieved with this microscope to detect trace impurities.

Table 1
Synthesis' parameters of YAG:Ce^{3+}, Pr^{3+}, Cr^{3+} nanophosphors.

Sample	Ce^{3+} (mol%)	Pr^{3+} (mol%)	Cr^{3+} (mol%)	Ammonia (ml)	Annealing temperature (°C)	Dye (mg)
N1	0.1	0.1	Traces	–	900	–
N2	0.1	0.1	Traces	25	900	–
N3	0.1	0.1	Traces	–	1100	–
N4	0.1	0.1	Traces	25	1100	–
C1	0.1	0.1	Traces	–	900	0.6
C2	0.1	0.1	Traces	–	900	1.0
N11	0.1	–	Traces	–	900	–
N12	–	0.1	Traces	–	900	–
N21	0.1	–	Traces	25	900	–
N22	–	0.1	Traces	25	900	–
N31	0.1	–	Traces	–	1100	–
N32	–	0.1	Traces	–	1100	–
N41	0.1	–	Traces	25	1100	–
N42	–	0.1	Traces	25	1100	–

2.3. Optical characterization

The emission spectra of samples were obtained under 340 nm or 460 nm excitation wavelengths from a Xenon Lamp of 75 W. The fluorescence emission was analyzed with an Acton Pro 3500i monochromator (Acton Research Corporation) and a R955 Hamamatsu photomultiplier tube for visible emission. The absorption spectra ranging from 200–800 nm were obtained from a Perkin-Elmer lambda 900 spectrometer. The IR spectra [Fourier transform infrared (FTIR)] of samples were recorded in the range of 400–4000 cm^{-1} on an ABA (MB300) spectrometer using the KBr pellet method. All optical measurements were carried out at room temperature.

2.4. Blue dye-impregnating procedure

Sample N1 annealed at 900 °C which presented the broadest visible emission under 340 nm excitation, was impregnated with the efficient blue dye Coumarin 480 in the following way: 0.6 mg of dye was dissolved in 20 ml of absolute ethanol, then 100 mg of the N1 sample was introduced in 10 ml of the solution and a strong stirring was carried out during 1 h. Afterwards, the solution was dried at 100 °C during 1 h and the powder was used to make a pellet (sample C1). A similar procedure was achieved to obtain another dye-impregnated YAG/YAM sample, but the initial solution was 1 mg of Coumarin in 20 ml of absolute ethanol (sample C2).

3. Results and discussion

3.1. Structural characterization

The characteristic XRD patterns of prepared samples are shown in Fig. 1. Such patterns show a mixture of cubic phase of YAG and monoclinic phase of YAM for samples annealed at 900 °C, according to JCPDS 33-0040 (YAG) and JCPDS 83-0935 (YAM) cards. The phase composition was estimated by the Rietveld iterative process. According to this, the phase composition was (YAG/YAM) 55/45 wt% and 63/37 wt% for samples prepared without (N1) and with (N2) ammonia, respectively, see Fig. 1a and b. The increment of annealing temperature to 1100 °C stabilizes completely (100 wt%) the YAG crystalline phase for both N3 and N4 samples as described in Fig. 1c. Then, it is reasonable to conclude that the introduction of ammonia helps to stabilize the YAG crystalline phase at 900 °C. Ammonia could be considered as a fuel that introduces additional energy to the system and then an increment of cubic phase. In fact, the increment of annealing temperature to 1100 °C stabilizes completely such crystalline phase. In addition, N11 has the same phase composition as that of N1, while N21 and N22 have the same composition as that of N2. This suggests that the content of dopant is not influencing the phase composition. The same situation was observed for N31 and N41, in whose case the phase composition is similar as that of N3 and N4. YAG is a cubic phase with space group Ia3d and cell parameter $a=12.01$ Å, while YAM is monoclinic with space group $P2_1/c$ and $a=0.7373$ nm, $b=1.0467$ nm, $c=1.1121$ nm, and $\beta=108.53°$. YAG shows dodecahedral, octahedral and tetrahedral sites, named A, B and C sites respectively. In this garnet, Y^{+} occupies the A site; therefore Pr^{3+} could take this place. In the case of YAM, the Y^{+} ion could be coordinated to six or seven oxygen atoms; thus, Pr^{3+} could occupy a six-coordinated center or seven-coordinated center.

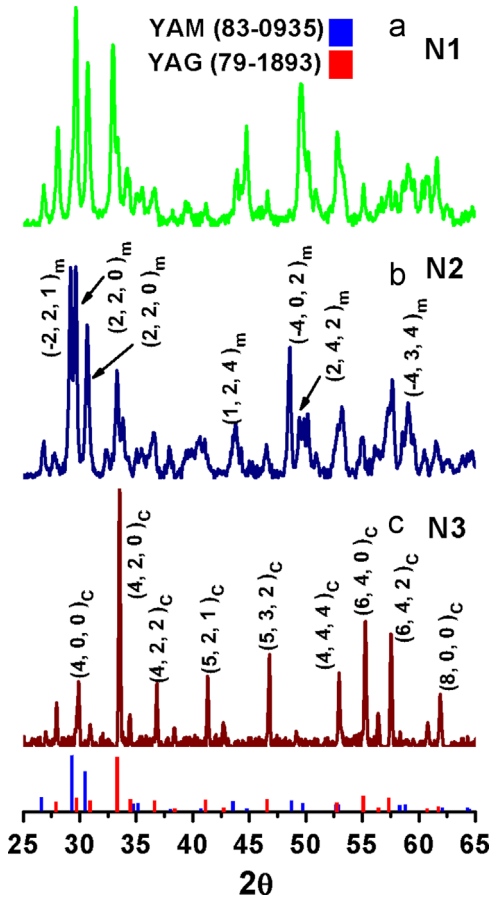

Fig. 1. XRD of nanopowder annealed at 900 °C and synthesized with (a) NaOH (N1), (b) NaOH+NH_4OH (N2), (c) NaOH annealed at 1100 °C (N3).

3.2. Morphology

According to HRTEM images, the average particle size of N1 and N2 is 50 nm, see Fig. 2. A careful analysis of HRTEM images suggests that such nanoparticles are the result of the agglomeration of small nanocrystals as shown in Fig. 2 for sample N1; a similar behavior was observed for N2. The growth mechanism of these nanoparticles is as follows: In the first stage of the synthesis, nanoparticles of 2 nm are obtained as shown in Fig. 2a; the inset shows the fast fourier transform (FFT) showing the crystalline nature. These nanocrystals act as a seed, which in turn self-ensemble forming an irregular agglomerate of nanocrystals as clearly observed in Fig. 2b. Such nucleation grows along time in a disordered manner to form big polycrystalline particles; Fig. 2c shows a stage growing at approximately 11 nm. The inset shows the FFT confirming the crystalline nature of the particle. Furthermore, the HRTEM image from Fig. 2c is shown in Fig. 2d and an interplanar separation of 2.54 Åwas measured. Those polycrystalline particles keep nucleation growing to form a final polycrystalline nanoparticle of 50 nm, see Fig. 2e. In this case, the HRTEM image shows an interplanar separation of 2.81 Å in Fig. 2f. Such distortion is probably associated to the irregular aggregation of nanocrystals.

3.3. Impurities

The FTIR spectra of samples N1, N2, N3 and N4 in Fig. 3a and b show a sharp band centered at 479 cm^{-1} which is attributed to the stretching vibrations of the AlO_4 tetrahedra, as well as two bands peaking at 732 cm^{-1} and 798 cm^{-1} which are associated to stretching vibration of the AlO_6 octahedra [10]. Also the peaks at 1016 cm^{-1}, 1464 cm^{-1}, and the band around 3474 cm^{-1} are attributed to CO_2 groups, bending vibration of OH groups from the residual adsorbed water, and stretching vibration of OH groups adsorbed on the surface of YAG nanophosphors, respectively [10,12]. Moreover, Y–O vibrations correspond to the 460 cm^{-1} and 560 cm^{-1} bands [13]. By comparing the samples N1 and N2 annealed at 900 °C, it is noticeable that the amount of OH groups and CO_2 impurities did not change, indicating that the introduction of ammonia does not have an effect over the content of impurities on YAG/YAM:Ce^{3+}, Pr^{3+}, Cr^{3+} nanocrystals. Interestingly, the presence of ammonia diminishes the absorption of bands associated to AlO_6 octahedra suggesting a larger content of defects or distorted octahedral sites, see Fig. 3b. Nevertheless, the increment of annealing temperature increases such bands; see Fig. 3a, reducing defects and then increasing the symmetry of octahedral sites. Furthermore, a direct comparison between samples N1 and N3 suggests that the increment of annealing temperature reduces impurities, but the combined effect with the presence of ammonia reduces strongly the OHs content. Furthermore, combined effect strongly enhances the absorption bands of both tetrahedral and octahedral sites, suggesting that combined ammonia and higher annealing temperature contribute to a better binding between Al and O_2 atoms. In this way, a minimum of impurities and a pure YAG phase can be reached at lower temperatures than such employed in methods as solid-state reaction.

3.4. Optical properties

3.4.1. The fluorescent properties of YAG:Ce^{3+}, Pr^{3+}, Cr^{3+} under 460 nm excitation

The signal emitted of YAG/YAM:Ce^{3+}, Pr^{3+}, Cr^{3+} nanophosphors after excitation at 460 nm is shown in Fig. 4. The spectra shows a strong orange emission peak centered at 609 nm associated to the transition $^1D_2 \rightarrow {}^3H_4$ and two very weak bands at 640 nm and 670 nm associated to $^3P_0 \rightarrow {}^3H_6$ and $^3P_0 \rightarrow {}^3F_2$ of Pr^{3+}, overlapped with the strong green–yellow emission band of Ce^{3+} centered at 538 nm; this band is associated to the transitions from the lowest 5d levels of Ce^{3+} to $^2F_{5/2}$, $^2F_{7/2}$ levels. Such emission is in agreement with the results reported by other authors where a broad emission band going approximately from 520 nm to 580 nm has been observed [4,6,7,14]. Notice the strong increment of 83% in the integrated emission band (by comparing samples N1 and N2), see Fig. 4a, which could be partially associated with the stabilization of YAG crystalline phase changing from 55 wt% to 63 wt% as a result of the introduction of ammonia and annealing at 900 °C as discussed above. However, sample N3 had strong quenching of both Ce^{3+} and Pr^{3+} emissions while sample N4 had just quenching of Ce^{3+} emission regardless the 100 wt% of YAG crystalline phase. Furthermore, quenching of the Ce^{3+} emission is also observed even in the absence of Pr^{3+}, see Fig. 4b. In this case, a larger enhancement with the introduction of ammonia was observed, while little less quenching at high annealing temperature suggests that the phenomena associated to quenching effect depends on both active ions.

The luminescence quenching observed experimentally can be explained by the formation of Pr^{4+} and Ce^{4+}. It has been reported that Pr^{4+} ion is detrimental for the fluorescence emission because it promotes the formation of F color centers which act as a trap for electrons [15]. Those color centers are formed when the oxidation from Pr^{3+} to Pr^{4+} liberates an electron which is trapped in anionic vacancies; this in turn induces a charge compensation producing oxygen defects Vo. The experimental evidence of the formation of Pr^{4+} on samples N3 and N4 annealed at 1100 °C is based on the brown coloration of the samples; this change in color has been

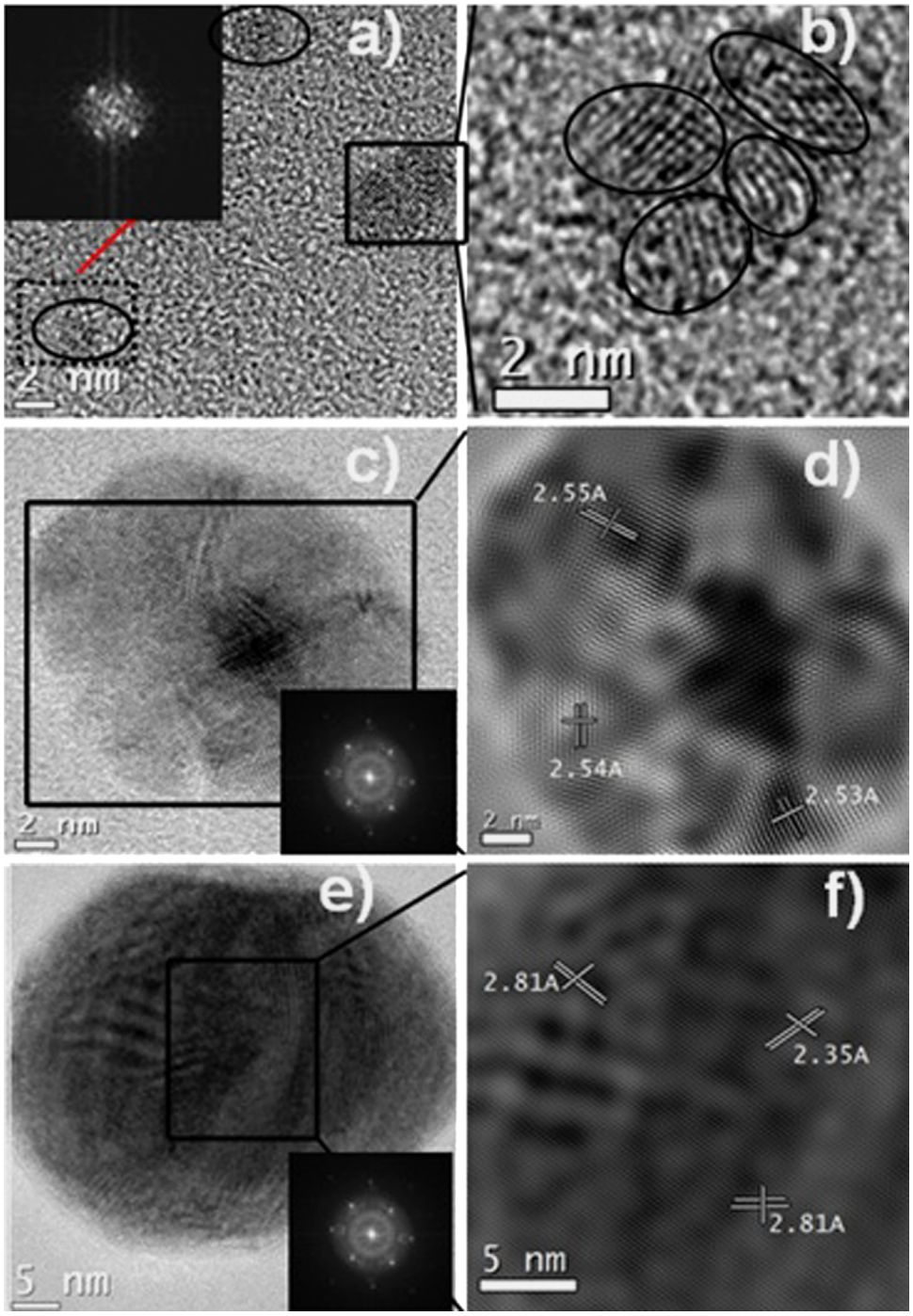

Fig. 2. Typical TEM and HRTEM images of sample N1 showing the seeds nanocrystals (a) and its agglomeration (b), which grows to form a larger particle (c). (d) and (f) are HRTEM images showing the interplanar distance of the particles formed with an ensemble of polycrystals (c,e). The insets show the fast Fourier transform (FFT) pattern for each stage of growing.

reported by other authors [16]. In addition, those samples presented broader absorption bands in comparison with samples annealed at 900 °C (N1 and N2), due to the superposition of F color centers, oxygen vacancies in the range of 500–700 nm and Pr^{4+} in the range of 300–570 nm as shown in Fig. 5 [15,17,18]. Furthermore, absorption spectra suggest that high annealing temperature promotes the formation of Pr^{4+} but the presence of ammonia avoids it. This can be corroborated by observing that sample N2 has a lower Pr^{4+} absorption band than that of sample N1 and also has a higher Pr^{3+} absorption band centered at 254 nm, see Fig. 5 [15]. Similar increment on such absorption band was also observed for sample N4 annealed at 1100 °C. Thus, Pr^{4+} is formed in all samples under study perhaps due to the specific characteristics of the synthesis process combined with the oxidative atmosphere where samples were annealed, promoted for a high annealing temperature and avoided with the presence of ammonia.

The absorption band at 254 nm related to Pr^{3+} was reduced in N3 in comparison with that of N4, and the bands at 464 nm and 510 nm associated to Ce^{3+} disappeared for N3 but remained for N4, as also shown in Fig. 5. This suggests the oxidation of Ce^{3+} to Ce^{4+} and Pr^{3+} to Pr^{4+} which is possible because the annealing was accomplished in an oxidizing environment. Such oxidation could partly explain the quenching of the signal emitted by Ce^{3+}

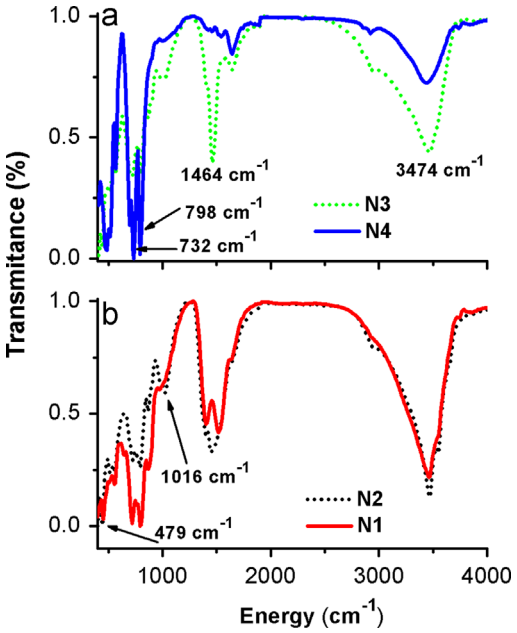

Fig. 3. FTIR spectra of (a) N3 and N4 samples annealed at 1100 °C, (b) N1 and N2 samples annealed at 900 °C.

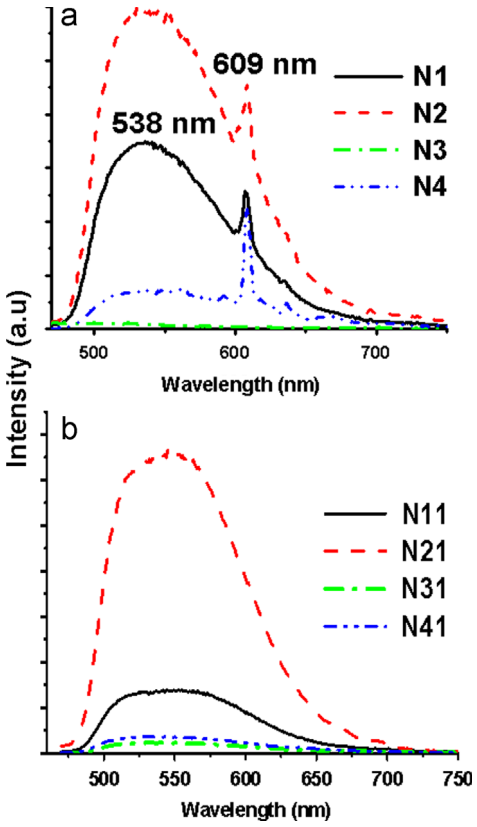

Fig. 4. Photoluminescence of (a) codoped Ce^{3+}, Pr^{3+} and (b) doped Ce^{3+}, both under 460 nm excitation.

in all samples, see Fig. 4a, and it was confirmed by the emission spectra of YAG:Ce^{3+} shown in Fig. 4b. In this case, samples were similarly prepared as those shown in Fig. 4a except that no Pr^{3+} was included. As observed, the emission of Ce^{3+} is quenched after annealing at 1100 °C, indicating the presence of oxidation from Ce^{3+} to Ce^{4+}. Notice the similar signal emitted for N31 and N41, and the larger increment with the presence of ammonia.

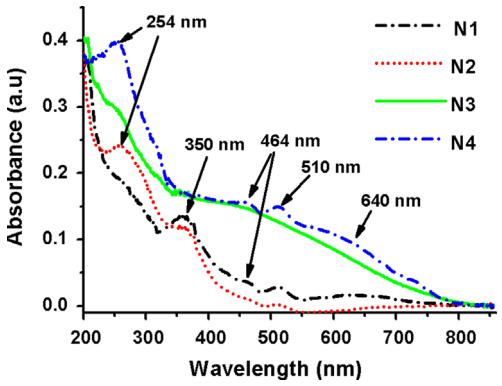

Fig. 5. Absorption spectra of samples N1–N4.

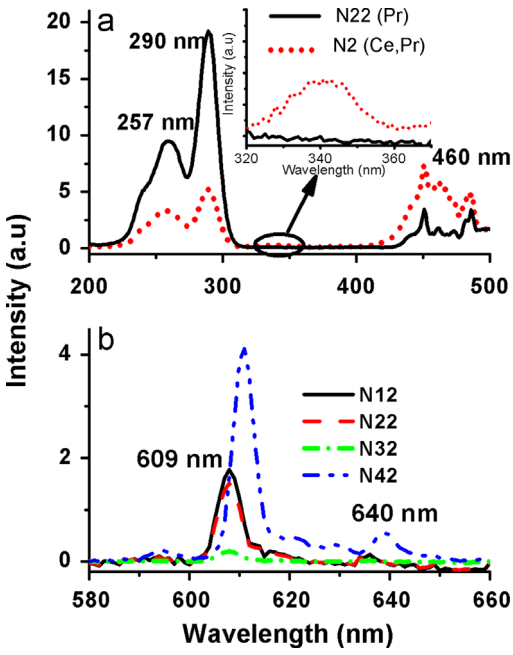

Fig. 6. (a) Excitation spectra of Pr^{3+} doped and Ce^{3+}, Pr^{3+} codoped at λ_{emi}=609 nm. The inset shows a close up of the marked area. (b) Photoluminescence of Pr^{3+} doped samples under 460 nm excitation.

In order to understand the emission mechanism under 460 nm excitation, a YAG/YAM:Pr^{3+} (N22) sample was prepared by using the same synthesis procedure than that of N2, except that Ce^{3+} was not included. Fig. 6a shows the excitation spectrum at λ_{emis}=609 nm for N22. Two Pr^{3+} excitation bands centered at 257 nm and 290 nm associated to $^3H_4 \rightarrow 4f^15d$ transition, and multiple peaks around 460 nm associated to $^3H_4 \rightarrow {}^3P_j$ transition were also observed. It is worthy to notice that the excitation band in the range of 220–310 nm includes the broad $5d_3$ band (located at around 37,000 cm^{-1}) of Ce^{3+} [6,19]. With the introduction of Ce^{3+} (N2), the excitation spectrum of YAG/YAM:Ce^{3+}, Pr^{3+}, Cr^{3+} at 609 nm shows broader 460 nm band due to the higher absorption cross section for Ce^{3+} and associated to the transition $^2F_{5/2} \rightarrow 5d_1$ overlapped with peaks associated to $^3H_4 \rightarrow {}^3P_j$ transition of Pr^{3+}. An additional weak band centered at 340 nm associated to the second 5d level ($5d_2$) transition of Ce^{3+} was also observed. Notice that both ions can be excited with 460 nm to produce emission at 609 nm, and only the presence of Ce^{3+} permits such red emission under excitation at 340 nm. Therefore, it is reasonable to conclude that 609 emission band of Pr^{3+} after 460 nm excitation is the result of both direct excitation and energy transfer

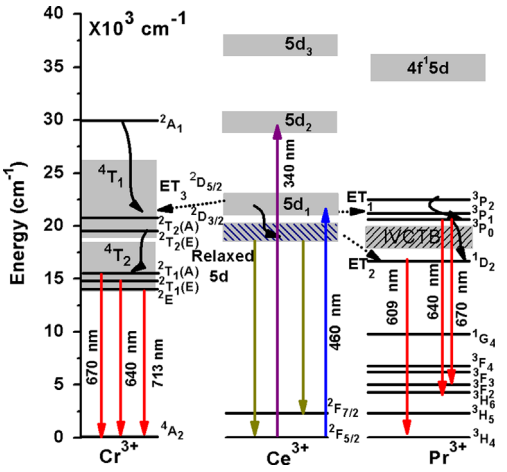

Fig. 7. Energy level diagram with the proposed mechanism of Ce^{3+}, Pr^{3+} and Cr^{3+} emissions.

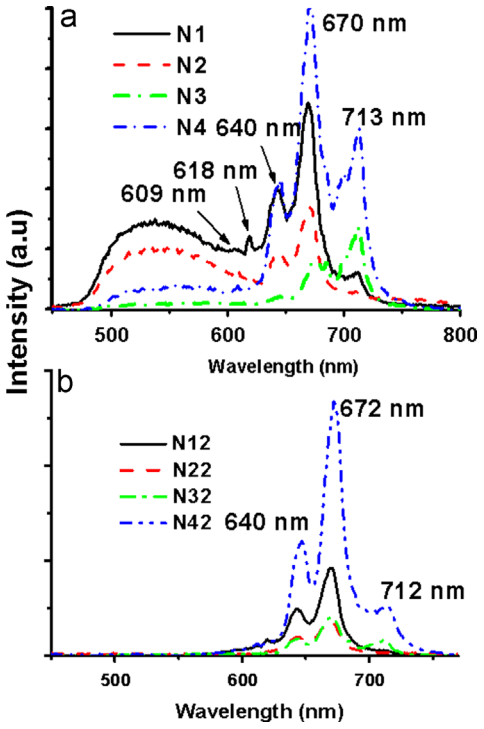

Fig. 8. Photoluminescence of (a) codoped Ce^{3+}, Pr^{3+}, Cr^{3+} and (b) doped Pr^{3+}, both under 340 nm excitation.

from Ce^{3+}, see Fig. 6b. In the former, $^3P_0$ is populated after excitation and then relaxed non-radiatively to $^1D_2$ that relaxes radiatively producing the 609 nm ($^1D_2 \rightarrow {}^3H_4$) emission band, and radiative relaxation $^3P_0 \rightarrow {}^3H_6$ producing weak emission band at 640 nm. Although the absence of the well-known emission band at 490 nm ($^3P_0 \rightarrow {}^3H_4$) can be explained by the re-absorption for Ce^{3+} in the codoped system, only a weak signal was observed in the Pr^{3+} doped samples suggesting the presence of defects quenching such emission. It has been postulated that quenching of 490 nm emission, and any other band associated to $^3P_0$ relaxation, is possible with the presence of intervalance charge transfer (IVCT) band located between $^3P_0$ and $^1D_2$ levels [20–22]. Such band could be composed of color centers or defects produced by charge compensation during the oxidation of Ce^{3+}, Pr^{3+} to Ce^{4+}, Pr^{4+}, or during the synthesis process. In this case, relaxation of population follows the scheme $^3P_0 \rightarrow$ IVCTB $\rightarrow {}^1D_2$, which explains why the dominant emission band is coming from $^1D_2$ energy level and only small population from $^3P_0$ relaxes radiatively to ground state. Transitions discussed above are displayed in the energy diagram of Fig. 7, and they are in correspondence with previous results reported in the literature [6,7,15,17,23].

In the energy transfer mechanism, Pr^{3+} can be excited either by a non-radiative energy transfer from the lowest part of 5d levels of Ce^{3+} to $^3P_0$ of Pr^{3+} (ET_1) or by a non-radiative energy transfer from relaxed 5d of Ce^{3+} to $^1D_2$ of Pr^{3+} (ET_2) as shown in Fig. 7. From those excited levels, the relaxation mechanism is similar as described above producing the 609 nm dominant band from Pr^{3+}. It is probable that both direct and energy transfer excitation occur. This explains the enhancement emission of Pr^{3+}, even though the emission of Ce^{3+} dominates the signal emitted; see emissions of N1 and N2 in Fig. 4a. Therefore, considering the excitation band at 340 nm for Ce^{3+} and the possibility to excite Pr^{3+} by energy transfer, it should be possible to get both yellow emission from Ce^{3+} and red emission from Pr^{3+} by exciting at 340 nm as will be discussed in the next section.

3.4.2. *The fluorescent properties of YAG:Ce^{3+}, Pr^{3+}, Cr^{3+} under 340 nm excitation*

Dominant broad red emissions overlapped with the yellow emission of Ce^{3+} were observed in all samples under study after excitation at 340 nm as shown in Fig. 8a. Interestingly, the red band is not dominated by the typical 609 nm emission associated to $^1D_2 \rightarrow {}^3H_4$ transition of Pr^{3+} as discussed above and only a weak signal of such band can be observed in the emission spectra. However, its presence confirms the energy transfer $Ce^{3+} \rightarrow Pr^{3+}$. The dominant band centered at 670 nm cannot be associated as typically to $^3P_0 \rightarrow {}^3F_2$ or $^1D_2 \rightarrow {}^3H_5$ because it requires population on $^3P_0$ and $^1D_2$ that in turn should dominate the signal emitted after radiative relaxation, as discussed above. In addition, the same spectra were obtained in the absence of Ce^{3+} (or Pr^{3+}) as shown in Fig. 8b suggesting that such radiative relaxation should be associated to some impurities introduced during the synthesis process.

Recently, it was reported that the red emission of Ce^{3+} can be enriched by codoping with Cr^{3+} with dominant emission bands peaking at 670, 685 and 700 nm [24]. Such bands are in agreement with those bands observed in our experiments, see Fig. 8, and therefore confirms the presence of Cr^{3+} impurities in our nanophosphor. Such impurities must be in the level of traces because they were not detected by EDS analysis. In our case, impurities came from the autoclave used for the preparation of nanocrystals as was confirmed by the preparation in a different container. The proposed mechanism for the excitation and relaxation of Cr^{3+} is shown in Fig. 7 and it can be described as follows. Although Cr^{3+} can be excited directly to $^2A_1$ energy band, it is possible that after excitation at 340 nm the $5d_2$ level of Ce^{3+} was populated and partially relaxed non-radiatively to $5d_1$ that in turn relaxes to ground state radiatively producing the green–yellow band centered at 538 nm. In addition, a non-radiative decay can occur from the $5d_1$ band of Ce^{3+} to $^4T_1$ and $^2T_2(E)$ energy bands of Cr^{3+} (ET_3) and then to $^4T_2$, $^2T_1(A)$, $^2T_1(E)$ and ^2E that relaxes to ground state $^4A_2$ producing the red emission band, see Fig. 7. Notice that the energy transfer from $5d_1(Ce^{3+})$ to $^2T_2(E)$ (Cr^{3+}) after excitation of 460 nm is also possible. Although the explanation of 672 nm dominant band is consistent with the experimental results, more studies are in progress to confirm the proposed mechanism that will be reported in a forthcoming paper.

The signal emitted is dominated by the red band but the yellow to red ratio (Y/R) was changed with the introduction of ammonia and the increment of annealing temperature. The Y/R for N1 was ~0.42 and changes to ~0.007 for N3 as a consequence of the complete stabilization of YAG crystalline phase. In this last case,

the signal emitted is dominated by the red band, opposite to excitation at 460 nm where the signal emitted of N3 disappears. As was observed previously, the introduction of ammonia enhances the red emission of Pr^{3+} under excitation at 340 nm as observed by comparing the ratios $Y/R \sim 0.59$ for N2 and $Y/R \sim 0.07$ for N4. Notice the strong enhancement of 670 nm emission band with the combined effect of ammonia and pure YAG crystalline phase. These experimental results confirm the important role of the ammonia and YAG/YAM phase composition. It suggests that Pr^{3+} emission is enhanced by YAG crystalline phase and that the presence of ammonia reduces the formation of Pr^{4+}. It is important to note that an adequate balance between yellow and red emissions was obtained for samples N1 and N2 where the YAM crystalline phase appeared.

On the other hand, the contribution of red emission under UV excitation can be controlled either by the addition of ammonia or annealing temperature as shown in Fig. 8a. This suggests that YAG:Ce^{3+}, Pr^{3+}, Cr^{3+} nanophosphors could be excellent candidate to generate white light under 340 nm excitation. As a proof of concept, a blue component was added and white light was obtained as discussed in the next section.

3.4.3. White light emission under 340 nm excitation

Several groups have reported very efficient LEDs emitting in the ultraviolet region at 340 nm for the study of organic molecules, biosensing applications and solid-state lighting [25–28]. For lighting applications, RGB phosphors are required; then the green–yellow–red emission of YAG:Ce^{3+}, Pr^{3+}, Cr^{3+} is very attractive for this application. In this section, it is discussed the white light generation obtained by using this nanophosphor impregnated with a Coumarin 480 blue dye. The emission spectra of sample N1 impregnated with a Coumarin(mg)/absolute ethanol(ml) in the ratio of 0.6/20 (Sample C1) and with a 1/20 ratio (Sample C2) under 340 nm excitation are shown in Fig. 9a. The CIE coordinates were (0.30,0.36) for sample C1, very near to the ideal coordinates (0.33, 0.33) for white light, see Fig. 9b. The CIE coordinate of sample C2 was (0.26, 0.28), little shifted to the blue region as a result of the dominant blue peak centered at 437 nm; therefore the emission observed by the naked-eyes was bluish-white. Coumarin presented an emission peak at 463 nm when it is dissolved in absolute ethanol (sample C3), but it has a shifting of 26 nm to shorter wavelengths when it is impregnated on nanophosphors. Such displacement in the emission peak from 463 nm to 437 nm is associated partly to the interaction of the Coumarin dye with the nanophosphor and partly is the blue absorption effect of Ce^{3+} and Pr^{3+}. Furthermore, the three component system is excited simultaneously; therefore the emission of Pr^{3+} decreases in C1 with respect to N1, since the excitation wavelength would be shared among three elements. Nevertheless, the emission of Ce^{3+} in C1 increases with respect to N1, suggesting that Ce^{3+} reabsorbs the emission at 463 nm from Coumarin. This confirms the shifting in the emission peaks of C1 compared to N1 produced by the reabsorption of Ce^{3+}.

In this particular system, only the blue emission could be controlled since the nanophosphors had a fixed concentration of 0.1 mol% for the Ce^{3+} and Pr^{3+}. Nevertheless, it is also possible to change the concentration of Ce^{3+} and Pr^{3+} or to add a controlled amount of Cr^{3+} to make a better change of CIE color coordinates. In this way, this system could be employed to create warm and cool white light sources by tailoring the concentrations of Ce^{3+}, Pr^{3+}, Cr^{3+} and the blue dye. Furthermore, it is necessary to find a replacement material for Coumarin since this colorant is bleached after prolonged exposure to UV excitation. Such material should provide good emission efficiency around 460 nm in order to improve the white light emission. The solution of all those problems is the objective of a current work that will be reported elsewhere.

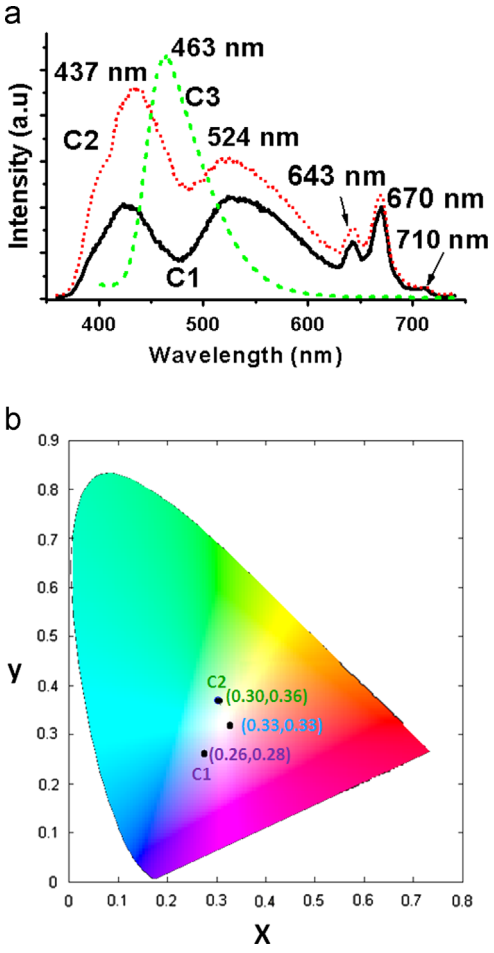

Fig. 9. (a) Photoluminescence spectra under 340 nm excitation of samples C1 (0.6 mg), C2 (1 mg) and Coumarin 480 (sample C3). (b) CIE coordinates of C1 and C2 samples.

4. Conclusions

Codoped YAG:Ce^{3+}, Pr^{3+}, Cr^{3+} nanophosphors with an average crystallite size of 50 nm were prepared by the precipitation method. The phase composition is strongly dependent on the component used for preparation and annealing temperature. 55 wt% of YAG crystalline phase was observed for samples annealed at 900 °C and increased to 63 wt% with the introduction of ammonia. Furthermore, the increase of annealing temperature up to 1100 °C stabilizes 100% the YAG crystalline phase with and without the presence of ammonia. However, such annealing temperature enhances the formation of Ce^{4+}, Pr^{4+} and color centers induced by the charge compensation. According to the experimental results reported here, defects located between $^3P_0$ and $^1D_2$ are responsible of the quenching of 490 emission characteristic of Pr^{3+}. The oxidation of Ce^{3+} and Pr^{3+} to Ce^{4+} and Pr^{4+}, and defects produced during the sample preparation are supported by the absorption spectra and confirmed by the quenching of the signal emitted even that YAG crystalline phase was stabilized at 100%. A broad red emission band overlapped to Ce^{3+} emission was produced under 340 nm excitation due to the presence of trace impurities of Cr^{3+}; this broad green–yellow–red emission band produced by the Ce^{3+}, Pr^{3+} and Cr^{3+} ions was used along with a blue dye to produce white light, which had CIE

coordinates (0.30, 0.36) close to ideal white. This demonstrates that the phosphor reported here is a good candidate to produce white light by combining the broad red emission of Pr^{3+} and Cr^{3+} with the blue emission from some organic or inorganic material.

Acknowledgment

We acknowledge CONACYT for financial support through Grant 134111 and for the PhD scholarship for J. Oliva and O. Meza.

References

[1] T. Mah, T.A. Parthasarathy, H.D. Lee, J. Ceram. Process. Res. 5 (2004) 369.
[2] H.S. Jang, Y.H. Won, D.Y. Jeon, Appl. Phys. B 95 (2009) 715.
[3] R. Mueller-Mach, G.O. Mueller, M.R. Krames, T. Trottier, IEEE J. Sel. Top. Quantum Electron. 8 (2002) 339.
[4] Y. Pan, M. Wu, Q. Su, J. Phys. Chem. Solids 65 (2004) 845.
[5] J.W. Lee, J.H. Lee, E.J. Woo, H. Ahn, J.S. Kim, C.H. Lee, Ind. Eng. Chem. Res. 47 (2008) 5994.
[6] H.S. Jang, W.B. Im, D.C. Lee, D.Y. Jeon, S.S. Kim, J. Lumin. 126 (2007) 371.
[7] H. Yang, Y.S. Kim, J. Lumin. 128 (2008) 1570.
[8] X. Yang, J. Liu, H. Yang, X. Yu, Y. Guo, Y. Zhou, J. Liu, J. Mater. Chem. 19 (2009) 3771.
[9] X. Zhang, J. Zhang, X. Zhang, L. Chen, Y. Luo, X.J. Wang, Chem. Phys. Lett. 434 (2007) 237.
[10] Y. Zhang, H. Yu, Ceram. Int. 35 (2009) 2077.
[11] H. Yang, L. Yuan, G. Zhu, A. Yu, H. Xu, Mater. Lett. 63 (2009) 2271.
[12] J. Wang, W. Miao, Y. Li, H. Yao, Z. Li, Mater. Lett. 63 (2009) 1794.
[13] R. Srinivasan, R. Yogamalar, Arumugam Chandra Bose, Adv. Sci. Lett. 2 (2009) 65.
[14] Y. Zhang, L. Li, X. Zhang, Q. Xi, J. Rare Earths 26 (2008) 446.
[15] D. Pawlak, Z. Frukacz, Z. Mierczyk, A. Suchocki, J. Zachara, J. Alloys Compd. 275 (1998) 361.
[16] A.P. Vink, P. Dorenbos, J.T.M de Haas, H. Donker, P.A. Rodnyi, A.G. Avanesov, C.W.E van Eijk, J. Phys.: Condens. Matter 14 (2002) 8889.
[17] N.A. Ivanov, V.D. Lokhnygin, A.A. Fomichev, V.M. Khulugurov, B.P. Chernyago, J. Appl. Spectrosc. 46 (1987) 207.
[18] Q. Zhang, T. Liu, J. Chen, X. Feng, Phys. Rev. B 68 (2003) 064101.
[19] H. Guo, H. Zhang, J.J. Li, F. Li, Opt. Express 18 (2010) 27257.
[20] P. Boutinaud, R. Mahiou, E. Cavalli, M. Bettinelli, J. Alloys Compd. 122–123 (2007) 430.
[21] P.J. Deren, R. Pazik, W. Strek, Ph Boutinaud, R. Mahiou, J. Alloys Compd. 451 (2008) 595.
[22] E. van der Kolk, P. Dorenbos, C.W.E. van Eijk, A.P. Vink, C. Fouassier, F. Guillen, J. Lumin. 97 (2002) 212.
[23] S. Zhou, Z. Fu, J. Zhang, S. Zhang, J. Lumin. 118 (2006) 179.
[24] L. Wang, X. Zhang, Z. Hao, Y. Luo, X.J. Wang, J. Zhang, Opt. Express 18 (2010) 25177.
[25] S.R. Jeon, M. Gherasimova, Z. Ren, J. Su, G. Cui, J. Han, H. Peng, Y.K. Song, A.V. Nurmikko, L. Zhou, W. Goetz, M. Krames, Jpn. J. Appl. Phys. 43 (2004) L1409.
[26] K. Davitt, Y.K. Song, W.R. Patterson III, A.V. Nurmikko, Opt. Express 13 (2005) 9548.
[27] H. Peng, E. Makarona, Y. He, Y.K. Song, A.V. Nurmikko, Appl. Phys. Lett. 85 (2004) 1436.
[28] J.S. Cabalu, A. Bhattacharyya, C. Thomidis, I. Friel, T.D. Moustakasa, J. Appl. Phys. 100 (2006) 104506.